




# Influence of SrTiO<sub>3</sub> on microstructure and electrical properties of Ca<sub>0.9</sub>Sr<sub>0.1</sub>Cu<sub>2.9</sub>Mg<sub>0.1</sub>Ti<sub>4</sub>O<sub>12</sub> ceramics

Salam Rhouma<sup>1,2,3,\*</sup> , Adel Megriche<sup>1</sup>, Mohamed El Amrani<sup>2</sup>, Senda Said<sup>1</sup>, and Cécile Autret-Lambert<sup>2</sup>

<sup>1</sup> Faculté des Sciences de Tunis, Université de Tunis El Manar, Unité de Recherche de Chimie Minérale Appliquée (UR11ES18), Campus Universitaire Farhat Hached, 2092 Tunis, Tunisia

<sup>2</sup> GREMAN, UMR 7341 CNRS, Université François Rabelais, UFR Sciences et Techniques, Parc de Grandmont, 37200 Tours, France

<sup>3</sup> Faculté des Sciences de Tunis, Laboratoire de Recherche de Chimie Minérale Appliquée (LR19ES02), Université de Tunis El Manar, Campus Universitaire Farhat Hached, 2092 Tunis, Tunisia

Received: 4 December 2022

Accepted: 12 February 2023

Published online:

7 March 2023

© The Author(s), under exclusive licence to Springer Science+Business Media, LLC, part of Springer Nature 2023

## ABSTRACT

In this work, a novel ceramic sample (1-x) Ca<sub>0.9</sub>Sr<sub>0.1</sub>Cu<sub>2.9</sub>Mg<sub>0.1</sub>Ti<sub>4</sub>O<sub>12</sub> (CSCMTO) – x SrTiO<sub>3</sub> (STO) (with x = 1, 3, and 10 weight%) was suggested by combining two oxide phases to create a new system. All the ceramic samples were prepared by solid-state reactions. The impact of the STO phase on the structure and dielectric properties of CSCMTO ceramic was analyzed through X-ray diffraction, scanning electron microscopy, Raman, and dielectric measurements. The increase in STO content brings about a decrease in mean grain size. The Raman and EDS measurements indicate the presence of STO and TiO<sub>2</sub> phases at grain boundaries. The dielectric constant values of ceramic samples range from 10<sup>3</sup> to 10<sup>4</sup>. They decrease progressively with the addition of the STO phase, accompanied by a reduction in the dielectric loss. The 0.9CSCMTO – 0.1STO reveals the lowest dielectric loss in the order of 0.031 at 10 kHz. Additionally, the STO phase plays a critical role in the enhancement of nonlinear properties. The 0.97CSCMTO-0.03STO shows the best value of breakdown voltage ( $E_b \approx 1820$  V/cm) as well as the highest nonlinear coefficient ( $\alpha \approx 3.55$ ). A heterogeneous microstructure with improved grain boundary properties was shown by impedance spectroscopy. The high grain boundary resistance is responsible for the reduced dielectric loss and improved breakdown voltage.

## 1 Introduction

Numerous research studies have been carried out to discover new materials with high dielectric permittivity [1]. Ceramic capacitors are well-known

examples of the application of materials due to the miniaturization of devices. Among them, the perovskite-like oxide CaCu<sub>3</sub>Ti<sub>4</sub>O<sub>12</sub> (CCTO) proved to be one of the best candidates because of its interesting dielectric constant  $\epsilon_r \approx 10^4$ – $10^5$  in a large

Address correspondence to E-mail: rhoumaa.salam@gmail.com

temperature [100–400 K] and frequency range [ $10^2$ – $10^6$  Hz] [2, 3]. Despite its giant dielectric constant, the CCTO shows a high dielectric loss and a low breakdown voltage compared to conventional ceramics like barium titanate or PZT, which limits its use in industrial applications [4]. Additionally, many factors can affect the dielectric properties of CCTO, like the preparation method, sintering temperature and time, doping ions, electrode materials [5–8]. On the other hand, numerous studies have been conducted, and many mechanisms have been proposed to explain the origin of the high dielectric constant of CCTO [9, 10]. The most widely accepted mechanism, known as the Internal Barrier Layer Capacitance (IBLC), consists of semiconducting grains and insulating grain boundaries. Moreover, the CCTO revealed a nonlinear current–voltage I–V property [3, 11, 12] that was brought about by the formation of double Schottky barriers at the grain boundaries [3, 7].

In general, increasing the barrier layer or grain boundary resistivity of CCTO is connected to decreasing dielectric loss (IBLC model). There are many ways to accomplish this, including adding cation doping ions in the CCTO lattice [13], changing Cu stoichiometry [14], filling oxygen vacancies at GBs. [5]. However, it is rarely seen that one of these methods reduces the dielectric loss while keeping a high dielectric constant.

The use of composite materials seems to be an interesting way to reduce dielectric losses while maintaining a suitable high dielectric constant. Anoop et al. [15] studied the effect of MgO on the CCTO phase, wherein they reported that the dielectric constant decreased to roughly 0.54 at 100 Hz while maintaining the high dielectric constant for a sintering time of 3 h only. Moreover, adding the STO phase has a good effect on promoting densification and enhancing the resistance of grain boundaries of CCTO. CCTO ceramics modified by SrTiO<sub>3</sub> were produced by H. Yu et al. [16] using a solid-state reaction technique. They discovered that adding a high STO ratio led to a significant reduction in the dielectric constant and CCTO losses.

In previous work [17], we investigated the effect of Sr and Mg doping ions on CCTO sintered for 12 h at 1100 °C. However, the Sr,Mg co-doped CCTO still faces issues with its relatively high dielectric loss (0.05) and long sintering time (12 h), both of which are undesirable for practical applications. The

objective of this study is to develop an effective method for reducing the sintering time and improving the overall dielectric characteristics of CCTO that has been co-substituted with Sr and Mg doping ions. The addition of a second phase to CCTO ceramics is one of the most successful approaches to dealing with this problem. As was previously indicated [16], STO has a favorable impact on reducing the dielectric loss. However, Peng et al. [18] reported a new ceramic system of  $(1-x)Y_{2/3}Cu_3Ti_4O_{12}-xSrTiO_3$ , and despite improvements in the dielectric constant and the breakdown voltage, considerable dielectric loss has been seen in these ceramics. Therefore, it is rare to find a dielectric ceramic material that satisfies the requirements for industrial applications, which include having a high dielectric constant with good frequency stability, low dielectric loss, and a high breakdown electric field. In this contribution,  $Ca_{0.9}Sr_{0.1}Cu_{2.9}Mg_{0.1}Ti_4O_{12}$  (CSCMTO)- $x$  SrTiO<sub>3</sub> (STO, with  $x = 0/1/3/10\%$ ) ceramic samples sintered at 6 h were successfully synthesized in this work using solid-state reaction. It was thoroughly explored how the STO phase affected the microstructure, dielectric, and nonlinear electrical properties of CSCMTO ceramic using different techniques. The dielectric properties and nonlinear J-E characteristics of the CSCMTO ceramics were both greatly enhanced by adding STO phases. The dielectric loss decreased progressively with the addition of the STO phase, and the 0.9 CSCMTO- 0.1 STO reveals the lowest value.

## 2 Experimental

$Ca_{0.9}Sr_{0.1}Cu_{2.9}Mg_{0.1}Ti_4O_{12}$  and  $(1-x) Ca_{0.9}Sr_{0.1}Cu_{2.9}Mg_{0.1}Ti_4O_{12} - x$  STO (where  $x=1/3/10\%$ ) (designed as CSCMTO, and  $(1-x)$  CSCMTO- $x$  STO, respectively) were prepared by traditional solid-state reaction method. CaCO<sub>3</sub> (99.9% purity), CuO (99.9% purity), TiO<sub>2</sub> (99.9% purity), SrCO<sub>3</sub> (99.9% purity), and MgO (99.5% purity) were used as starting raw materials to synthesize CSCMTO. The weighed raw materials were first mixed using a mortar and pestle before being ball-milled for 6 h in ethanol using a zirconia ball. The milled mixture was dried at 80 °C in an oven and calcined in the air at 1000 °C for 24 h, resulting in a brown powder. For the STO phase, the same procedure was used to combine TiO<sub>2</sub> and SrCO<sub>3</sub> in stoichiometric proportions before being

heated to 1200 °C for 12 h of calcination. The resultant powders (CSCMTO and STO) were again ground by ball-milling.

In the second step, the composite samples were prepared by mixing both CSCMTO and STO at stoichiometric ratios (1, 3, and 10% of the weight of STO). The mixed powders were pressed into disks of 10 mm in diameter and 2 mm in thickness by uniaxial compression at 300 bars. The disks were then sintered for 6 h at 1100 °C in the air.

The sintered pellets were first characterized by X-ray diffraction (XRD), using a D8 Bruker with CuK $\alpha$  radiation ( $\lambda = 1.540 \text{ \AA}$ ) over  $2\theta$  range of 20–80° with a step size of 0.02 and a step time of 12 s, to assess the phase composition of the synthesized ceramic samples. To investigate the microstructure of surface pellets, we used a Scanning Electron Microscopy (SEM) Hitachi 4160-F. Raman spectra were recorded at room temperature with a Renishaw inVia Reflex Raman Microscope using 514 nm as the exciting wavelength. In regards to dielectric measurements, the pellet surface was polished, and silver was sputtered onto either side of the pellet. The dielectric and complex impedance measurements were performed by an Agilent 4294 A impedance analyzer at room temperature in a frequency range from 100 Hz to 10 MHz. An Agilent B2911A device was used to evaluate the resistivity of ceramic samples at room temperature.

### 3 Results and discussion

The XRD patterns of the (1-x) CSCMTO + x STO (with  $x = 0/1/3/10\%$ ) ceramic samples, measured at room temperature, are presented in Fig. 1. All diffraction peaks can be matched with the standard CCTO configuration (JCPDS 75–2188), revealing that all ceramics present a cubic perovskite-related structure. In regard to three selected ceramics, it can be seen the presence of an extra peak characteristic of the STO phase, whose intensity increased progressively with the addition of value  $x$ .

The SEM micrographs presented in Fig. 2 highlight the evolution of grain size for each ceramic sample ((1-x) CSCMTO + x STO with  $x = 0/1/3/10\%$ ). The bulk density values are displayed in Table 1 and were determined by measuring the mass and (diameter/thickness) of the pellets. All the microstructures revealed a bimodal grain and the number of big

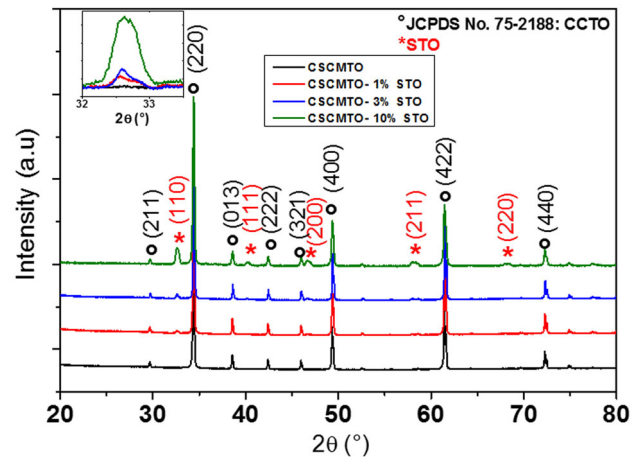


**Fig. 1** X-Ray diffraction patterns of (1-x) CSCMTO - x STO (with  $x = 0/1/3/10\%$ ) sintered at 1100 °C/6 h

grain sizes for 1, and 3% of STO are more important than CSCMTO. However, the ceramic with 10% STO showed a discernible decline. This variation is similar to that seen in CCTO ceramics doped with Sr<sup>2+</sup> [19]. Additionally, there are several clusters of tiny white grains that are joined by darker grains. EDS and Raman measurements were then used to identify these kinds of grains. On the other hand, it is difficult to distinguish between the sizes of composites with a low ratio of STO, but the number of large grains (10–12  $\mu\text{m}$ ) is more important for 1 weight.%. These results imply the possibility of an atomic inter-diffusion between STO and CSCMTO, as reported by Xue et al. [20]. Moreover, small grains intensified with the addition of the STO phase. This might be explained by increasing the interface thickness (between adjacent grains), which would minimize the insertion of Sr in the lattice and limit the grain boundary mobility of CCTO. Sintering at 6 h shows remarkable relative densities (95 and 96%). The best ceramic was 0.97 CSCMTO-0.03 STO (96.12%). These high values can result in an improvement in ceramic resistivity.

The EDS technique was carried out to clarify the elemental composition of tiny white grains in three studied ceramics. Table 2 shows all the atomic percentages of all the elements seen in different parts of ceramic samples. According to Table 2, it can be seen that the presence of Sr and Ti ions predominated strongly in different selected regions. These could be attributed to the SrTiO<sub>3</sub> phase.

To more clearly depict the distribution of the STO phase in the CSCMTO microstructure, it is crucial to

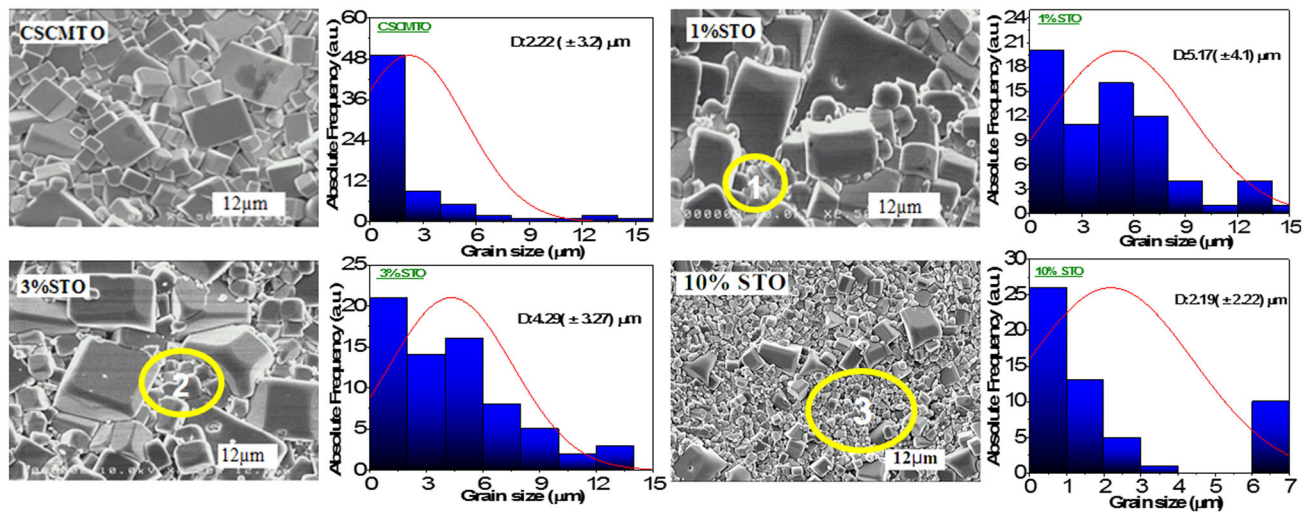


**Fig. 2** SEM images of surface morphologies of CCTO and (1-x) CSCMTO - x STO (with  $x = (0/1/3/10\%)$ ) sintered at 1100 °C/6 h with their grain size distributions and their mean grain sizes

**Table 1** The densities of (1-x) CSCMTO- x STO (with  $x = (0/1/3/10\%)$ )

	CSCMTO	CSCMTO-1% STO	CSCMTO-3% STO	CSCMTO-10% STO
D (%)	87.62	95.75	96.12	87.34

understand the composition of both grains and grain boundaries. Raman spectra measurements were used on grain Fig. 3a and grain boundaries Fig. 3b for two selected composites in the frequency range 100–1000  $\text{cm}^{-1}$ .

As seen in Fig. 3a, the grains showed the presence of peaks characteristic of the CCTO phase as reported in the literature [21, 22]. One peak with low intensity was detected at 286.5  $\text{cm}^{-1}$  ( $F_g$ ), and the others were observed at 444  $\text{cm}^{-1}$  ( $A_g$ ), 512  $\text{cm}^{-1}$  ( $A_g$ ), and 574  $\text{cm}^{-1}$  ( $F_g$ ). Additionally, the STO phase can be observed, which is represented by two broad bands

**Table 2** EDS analysis for Ca, Sr, Cu, Mg, and Ti atomic ratios pointed to regions 1, 2, and 3 of three selected ceramics (1, 3, and 10% STO).

Ceramic samples	Ca At (%)	Sr	Cu	Mg	Ti
1% STO					
Region 1	3.5	12.3	6.1	0.01	19.5
3% STO					
Region 2	4.24	15.2	6.6	0.1	24.2
10% STO					
Region 3	3.45	13.2	4.1	0.06	26.2

with their centers at low and high frequency ranges [200–400  $\text{cm}^{-1}$ ] and [600 and 800  $\text{cm}^{-1}$ ], respectively [23, 24]. The small particles seen in yellow circles on SEM micrographs are attributable to the STO phase. On the other hand, an additional peak relative to the  $\text{TiO}_2$  phase appeared at 600  $\text{cm}^{-1}$ , suggesting the chemical interaction between the two powders, CCTO and STO. This phenomenon was also observed in  $(\text{Ba}_{0.6}\text{Sr}_{0.4})\text{TiO}_3$  BST-CCTO [25], (1-x) CCTO - x  $\text{SrFe}_{12}\text{O}_{19}$  [26] et  $\text{Al}_2\text{O}_3$ -CCTO [27].

Figure 4 displays the dielectric constant and losses of all ceramic samples at room temperature (RT) as a function of frequency over the range from  $10^2$  to  $10^7$  Hz. All the values of dielectric response are summarized in Table 3. The dielectric constant of CSCMTO was significantly influenced by STO, as can be shown in Fig. 4a. The 0.99 CSCMTO-0.01 STO ceramic exhibits the highest dielectric constant in the order of 13,078 measured at 10 kHz. However, the dielectric constant decreases with further STO addition. As reported by previous literature, this change is comparable to that found in the CCTO ceramics doped with  $\text{Sr}^{2+}$  ions [19]. According to the SEM results, the 0.99 CSCMTO-0.01 STO ceramic also reveals the highest mean grain size. Moreover, similar patterns can be seen in the variations of the mean grain size and dielectric constant of all ceramics

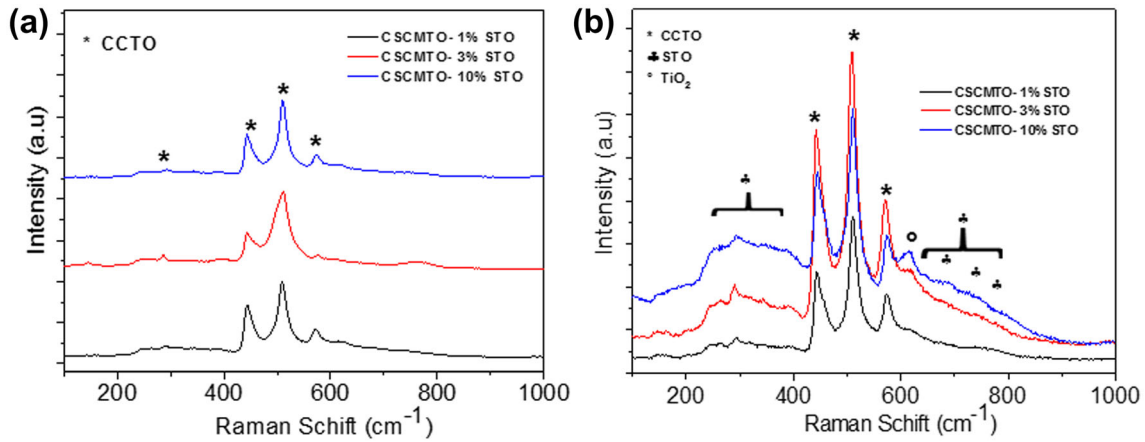


Fig. 3 Raman spectra on grains (a) and grain boundaries (b) of three selected composites

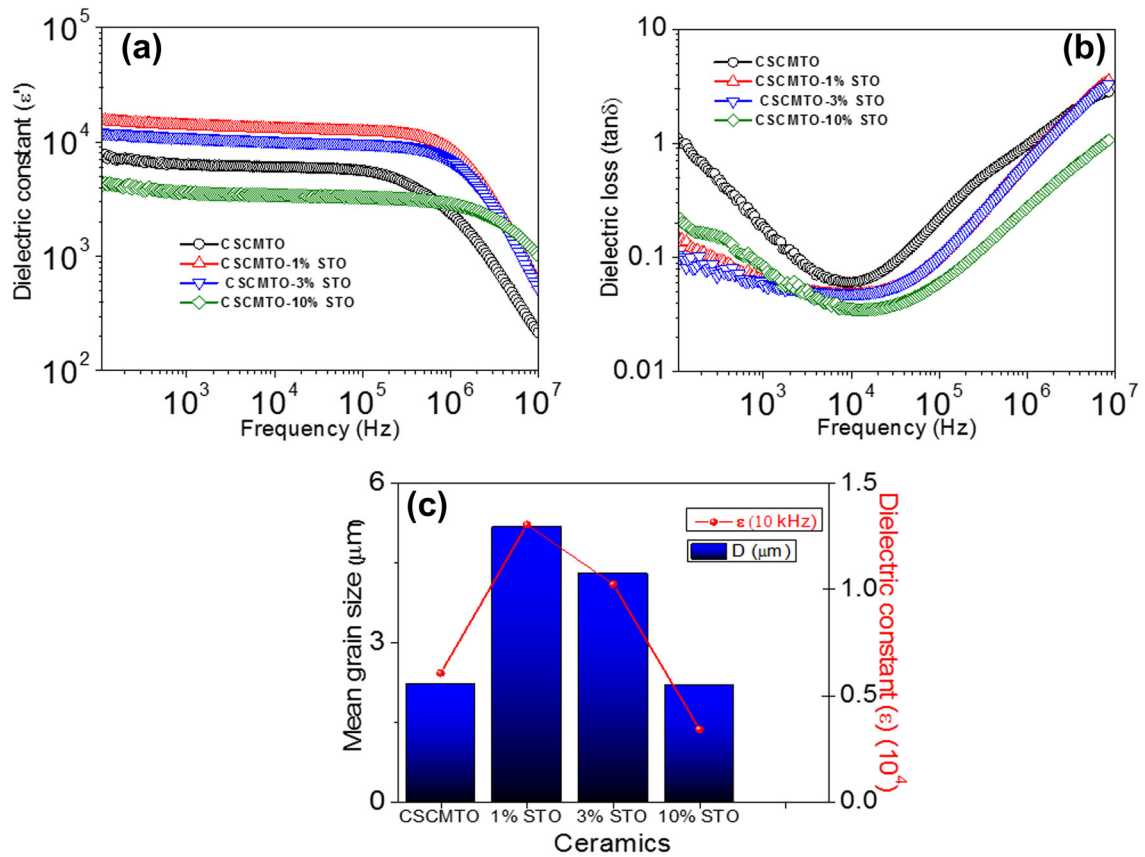


Fig. 4 Dielectric constant (a) and losses (b) of CCTO and (1-x) CSCMTO - x STO (with x= (0/1/2/3%)) sintered at 1100 °C/6 h. c Correlation between the dielectric constant ( $\epsilon'$ ) and the mean grain size of sintered ceramic samples

(Fig. 4c). This confirms a relationship between the permittivity and the mean grain size of CCTO [28]. This phenomenon is related to the IBL model, wherein the CCTO ceramic consists of grains and grain boundaries that behave like a semiconductor

and insulator, respectively. Thus, the dielectric constant can be expressed as the following Eqs. [29, 30]:

$$\epsilon_r = \epsilon_{gb}(A/t_{gb})$$

where  $\epsilon_r$ ,  $\epsilon_{gb}$ ,  $A$  and  $t_{gb}$  are the effective dielectric permittivity, the dielectric permittivity of the grain

**Table 3** Dielectric properties, parameters extracted from the RC model:  $R_g$ ,  $R_{gb}$ ,  $C_g$  and  $C_{gb}$  resistivity ( $\rho$ ), Nonlinear coefficient  $\alpha$ , breakdown down voltage ( $E_b$ ),

	$(\epsilon)$	$\tan(\delta)$	$R_g$ ( $\Omega$ )	$R_{gb}$ ( $\Omega$ )	$C_g$ (F)	$C_{gb}$ (F)	$(\rho)$ ( $\Omega.cm$ )	$(\alpha)$	$E_b$ ( $V.cm^{-1}$ )
CSCMTO	6074	0.072	35.39	$2.77 \cdot 10^5$	$1.62 \cdot 10^{-7}$	$5.20 \cdot 10^{-9}$	$2.891 \cdot 10^6$	1.64	700
1%STO	13,070	0.047	6.5	$1.30 \cdot 10^6$	$2.40 \cdot 10^{-7}$	$2.00 \cdot 10^{-8}$	$2.782 \cdot 10^7$	3.03	1075
3%STO	10,260	0.043	7.4	$1.62 \cdot 10^6$	$4.00 \cdot 10^{-7}$	$1.70 \cdot 10^{-8}$	$1.110 \cdot 10^8$	3.55	1820
10% STO	3423	0.031	8.03	$1.10 \cdot 10^6$	$1.00 \cdot 10^{-07}$	$3.90 \cdot 10^{-09}$	$3.907 \cdot 10^7$	1.67	850

boundary (GB), an average grain size, and the thickness of GB, respectively.

Additionally, this decrease could be explained by Lichtenecker's logarithmic law [31], showing that an increase in the volume fraction of STO contributes to a decrease in the dielectric constant as described in the following equation:

$$\ln \epsilon_{cal} = (1 - x) \ln \epsilon_{CCTO} + x \ln \epsilon_{STO}$$

where  $\epsilon_{cal}$ ,  $\epsilon_{CCTO}$  and  $\epsilon_{STO}$  are calculated, CCTO and STO dielectric constant, respectively.

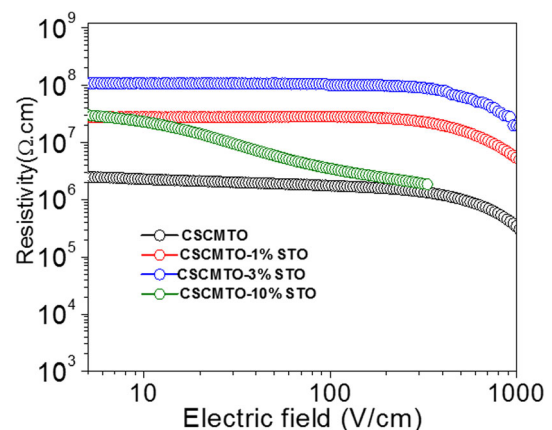
Moreover, the frequency stability of all ceramic samples was enhanced compared to CSCMTO and remains constant until  $10^6$  Hz, while it drops rapidly at higher frequencies [32, 33]. This phenomenon is related to the dielectric relaxation process [34, 35]. H.Yu et al. [16], synthesized CCTO ceramics modified by  $SrTiO_3$  and reported that adding a high percentage of STO (> 20%) causes a decrease in the dielectric constant of CCTO. It is true that our results show the same trend, but permittivity values are more important than those of their compounds.

As seen in Fig. 4b, the dielectric loss of ceramic composites reduced when STO phase was added and exhibit desirable values at low frequencies, such as 0.031 at 10 kHz (Table 3). According to the previous work, these values are lower than those observed by Peng et al. [18] and Mao et al. [36]. The restriction of DC conduction in the ceramics might be the cause of the low values of low-frequency dielectric loss. The results are consistent with what Y. Hu et al. [16] found. We were able to reduce it in our study by a little amount of STO, which is 40 times less than those shown in [16]. The change in dielectric loss is also influenced by relative densities. As a result, the reduction in dielectric loss may be explained by the thickening of the barrier layer at the grain boundary brought on by an increase in the STO ratio. According

to previous works, synthesis with the solid-state reaction method requires a high sintering time [9]. Our approach led to optimal dielectric properties in just six hours.

All ceramic samples' variations in resistivity as a function of electric field are depicted in Fig. 5. In comparison to CSCMTO ceramic, the ceramic samples reveal the highest resistivity values. Notably, the resistivity value of 0.97 CSCMTO-0.03 STO was increased by 20 orders of magnitude with respect to that of the CSCMTO ceramic. Thus, the enhancement of resistivity values could be related to the disappearance of the movement of charge carriers, which results in a decrease of dc conductivity and likewise the dielectric loss observed at lower frequencies [37]. Also, it can be found that the STO phase has a good impact on the stability of the resistivity compared to MgO and  $MgTiO_3$  reported in [15, 38].

In order to know separately the contribution of grains and grain boundaries, an equivalent circuit model has been proposed to explain the dielectric properties of CCTO. It is constituted by two parallel

**Fig. 5** Resistivity measurements of ceramic samples as a function of the electric field

RC elements connected in series (Fig. 6a). According to the IBLC model, one RC element corresponds to semiconducting grains ( $R_g, C_g$ ) and the second one to insulating grain boundaries ( $R_{gb}, C_{gb}$ ), as deduced from spectroscopy impedance [39].

Theoretically, the ideal impedance spectrum looks like the plane diagram model in Fig. 6a, with the grain resistance represented by a small semicircular arc and the grain boundary resistance by a wide semicircular arc (a).

According to the equivalent circuit, the complex impedance  $Z^*$  can be calculated using the following equation [40]:

$$Z^* = Z' - jZ'' = \frac{R_{gb}}{1 + j\omega R_{gb}C_{gb}} + \frac{R_g}{1 + j\omega R_gC_g}$$

where  $C_{gb}$  and  $R_{gb}$  stand for the resistance and capacitance of the insulating grain boundaries,  $C_g$  and  $R_g$  are the resistance and capacitance of the grain.

The impedance spectroscopy plots of all ceramics are shown in Fig. 6b at room temperature. The inset figure (Fig. 6c) presents an expanded view of high-frequency data near the origin. A nonzero intercept on the  $Z'$  axis can be used to determine the  $R_g$  value, which is observed at high frequencies. While the  $R_{gb}$  value can be deduced from the diameter of a large semicircular arc on the impedance complex plane plot at low frequency. Due to the large electrical heterogeneity between the grains and grain boundaries, it is challenging to get both semicircular arcs in one impedance spectrum at room temperature, and only the  $R_{gb}$  semicircular arc can be observed. In order to calculate the values of the  $R_g, R_{gb}, C_g$  and

$C_{gb}$ , the impedance measurement data were fitted using the EIS spectrum analyzer software in accordance with the appropriate equivalent circuits. Additionally, we added a constant phase element (CPE) in the circuit to precisely fit the experimental data. All the parameters ( $R_g, R_{gb}, C_g, C_{gb}$ ) extracted from the RC element model are summarized in Table 3.

It is obvious that STO phase has a great impact on the  $R_{gb}$ . For example, the ceramic with a weight of 3% STO shows the highest value, increasing by 5 orders of magnitude with respect to that of CSCMTO. Additionally, all the values are consistent with the variation in dielectric loss. On the other hand, it appears that the primary criteria for raising the  $R_{gb}$  values are a reduction in grain size and an improvement in grain boundary density. Our earlier research [41] indicated that the  $TiO_2$  phase might also help to enhance the  $R_{gb}$ . The  $R_g$  values of the chosen composites are almost constant but somewhat different from those of CSCMTO ceramic. This difference could be caused by the insertion of  $Sr^{2+}$  into the lattice of CSCMTO.

Thus, it is reasonable to conclude that grain and grain boundaries behave like semiconducting grains and isolating grain boundaries, thereby confirming the IBLC model.

Moreover, it was revealed that there is a relationship between the dielectric constant at low frequency and the capacitance of the grain boundary ( $C_{gb}$ ) as described in the following equation [42]:

$$\epsilon_r = C_{gb}/C_0$$

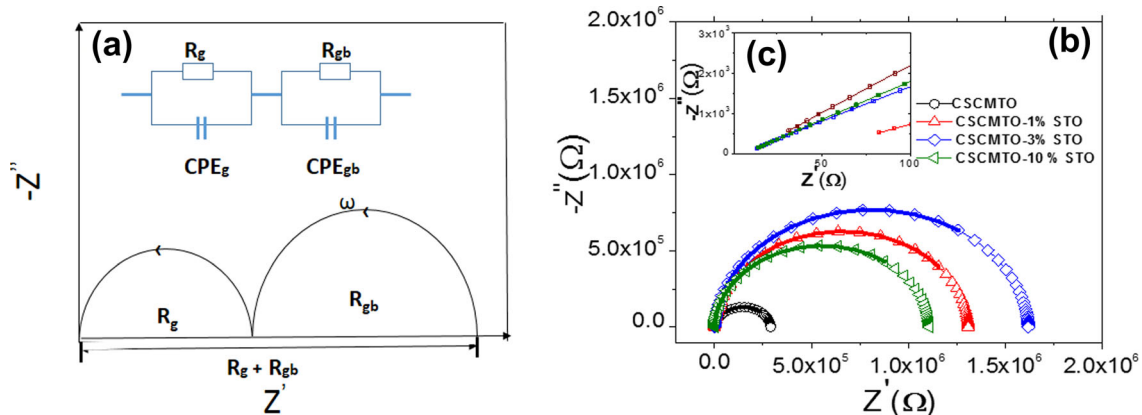


**Fig. 6** **a** Equivalent electric circuit consisting of two parallel RC elements connected in series. **b** Impedance complex plane plot ( $z^*$ ) at 25 °C for ceramic samples **c** shows an expanded view of the high frequency data close to the origin

where  $C_0$  is the empty cell capacitance. As a result, the decrease in dielectric constant of ceramic composites can be related to the decrease of  $C_{gb}$ . To sum up, the dielectric response is mainly governed by the grain boundary.

Figure 7 shows the nonlinear (J-E) characteristic of ceramic samples at room temperature to investigate the effect of STO on the electrical response of grain boundaries. The curves (J-E) displayed in Fig. 7 indicate that  $E_b$  values can be easily controlled for the grain boundary behavior with the addition of STO ratio. All the  $E_b$  values were obtained from this equation [43]:

$$E_{b(1mA)} = U_{(1mA)}/d$$

where  $U_{(1mA)}$  is the voltage corresponding to a current of 1 mA, and  $d$  is the thickness of the ceramic. While the nonlinear coefficient  $\alpha$  value was extracted from this formula:

$$\alpha = 1/[\log(U_{1mA}/U_{0.1mA})]$$

The obtained  $\alpha$  and  $E_b$  values are recapitulated in Table 3. The overall non-Ohmic results revealed that  $\alpha$  and  $E_b$  values increased with the addition of the STO ratio. The increase in  $E_b$  values is attributed to the enhancement of  $R_{gb}$  and the reduction of grain size and losses. Additionally, the obtained  $E_b$  values are higher than those obtained with MgO [44] and  $Al_2O_3$  [45], indicating an important effect of STO on the enhancement of the electrical properties of grain boundaries. On the other hand, the variation of  $\alpha$  can be explained by the Schottky-type barrier at the grain boundary [46]. Thus, the increase in  $\alpha$  as reported in [47, 48] may be due to the increase in Schottky barrier height resulting from

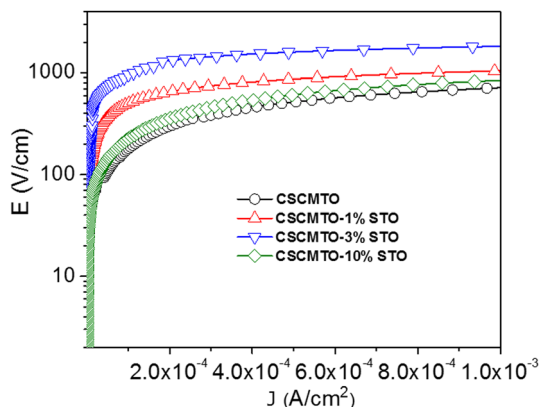


**Fig. 7** Nonlinear current-voltage behavior of ceramics samples sintered at 1100 °C/6 h

the improvement of  $E_b$ . Moreover, it can be seen that the (J-E) characteristic of 10% STO is similar to that of CSCMTO. According to Table 1, the relative density for 10% STO was lower than for 1 and 3% STO, which approximately equaled the value of CSCMTO. Besides, porosity can affect the  $E_b$  of CCTO. Therefore, the larger porosity observed for 10% STO results in lower  $E_b$  values, suggesting that porosity might impair the dielectric material's electrical performance.

To sum up, compared to the results found in  $Ca_{1-x}Sr_xCu_{2.9}Mg_{0.1}Ti_4O_{12}$  ceramics synthesized in our previous study, the STO phase resulted in a decrease in the dielectric loss as well as an increase in the breakdown voltage with a short sintering time.

## 4 Conclusion

The effect of STO addition on the microstructure, dielectric, and electrical properties of CSCMTO ceramic, prepared by the conventional solid-state reaction method, was systematically investigated. All ceramic samples show a relatively dense microstructure. The EDS and Raman results show the presence of STO and  $TiO_2$  phases at the grain boundary. The grain size decreases as the STO phase increases. A small amount of STO phase can significantly modify the dielectric and electrical properties of CSCMTO. All the ceramic samples reveal a high dielectric constant that varies from roughly  $10^3$ – $10^4$ . At 10 kHz, the 0.9CSCMTO – 0.1STO presents the lowest dielectric loss in the order of 0.031. Furthermore, the 0.97 CSCMTO-0.03 STO ceramic reveals a significantly improved electrical breakdown voltage value ( $E_b \approx 1820$  V/cm), a higher nonlinear coefficient of around ( $\alpha \approx 3.55$ ), and a higher grain boundary resistance ( $R_{gb} \approx 1.62 \cdot 10^6 \Omega$ ) value. The impedance spectrum analysis shows that the dielectric response is mainly governed by the grain boundary.

## Acknowledgements

This work was supported by a Tunisian Ministry of Higher Education Scholarship.

## Author contributions

SR: Conceptualization, methodology, visualization, writing—original draft, preparation, formal analysis,



and investigation. AM: Project administration, and writing—review. ME: Investigation. SS: Investigation. CA: Project administration, and writing—review.

## Funding

This work was supported by a Tunisian Ministry of Higher Education Scholarship

## Data availability

The datasets used or analyzed during the current study are available from the corresponding author on reasonable request.

## Declarations

**Conflict of interest** The authors declare that they have no known competing financial interests or personal relationships that could have appeared to influence the work reported in this paper.

## References

1. S. Krohns, P. Lunkenheimer, S. Meissner, A. Reller, B. Gleich, A. Rathgeber, T. Gaugler, H.U. Buhl, D.C. Sinclair, A. Loidl, The route to resource-efficient novel materials. *Nat. Mater.* 10, 899–901 (2011)
2. A.P. Ramirez, M.A. Subramanian, M. Gardel, G. Blumberg, D. Li, T. Vogt, S.M. Shapiro, Giant dielectric constant response in a copper-titanate. *Solid State Commun.* 115, 217–274 (2000)
3. S.Y. Chung, I.D. Kim, S.J.L. Kang, Strong nonlinear current–voltage behaviour in perovskite-derivative calcium copper titanate. *Nat. Mater.* 3, 774–778 (2004)
4. D. Xu, K. He, R. Yu, L. Jiao, H. Yuan, X. Sun, G. Zhao, H. Xu, Effect of AETiO<sub>3</sub> (AE = mg, ca, Sr) doping on dielectric and varistor characteristics of CaCu<sub>3</sub>Ti<sub>4</sub>O<sub>12</sub> ceramic prepared by the sol–gel process. *J. Alloys Compd.* 592, 220–225 (2014)
5. R. Yu, H. Xue, Z. Cao, L. Chen, Z. Xiong, Effect of oxygen sintering atmosphere on the electrical behavior of CCTO ceramics. *J. Eur. Ceram. Soc.* 32, 1245–1249 (2012)
6. J. Yang, M. Shen, L. Fang, The electrode/sample contact effects on the dielectric properties of the CaCu<sub>3</sub>Ti<sub>4</sub>O<sub>12</sub> ceramic. *Mater. Lett.* 59, 3990–3993 (2005)
7. T.B. Adams, D.C. Sinclair, A.R. West, Characterization of grain boundary impedances in fine- and coarse-grained CaCu<sub>3</sub>Ti<sub>4</sub>O<sub>12</sub> ceramics. *Phys. Rev. B: Condens. Matter.* 73, 094124 (2006)
8. Y. Yang, X. Wang, B. Liu, CaCu<sub>3</sub>Ti<sub>4</sub>O<sub>12</sub> ceramics from different methods: microstructure and dielectric. *J. Mater. Sci: Mater. Electron.* 25, 146–151 (2014)
9. M.A. Subramanian, D. Li, N. Duran, B.A. Reisner, A.W. Sleight, High dielectric constant in ACu<sub>3</sub>Ti<sub>4</sub>O<sub>12</sub> and ACu<sub>3</sub>Ti<sub>3</sub>FeO<sub>12</sub> phases. *J. Solid State Chem.* 151, 323–325 (2000)
10. B. Shri Prakash, K.B.R. Varma, The influence of the segregation of Cu-rich phase on the microstructural and impedance characteristics of CaCu<sub>3</sub>Ti<sub>4</sub>O<sub>12</sub> ceramics. *J. Mater. Sci.* 42, 7467–7477 (2007)
11. S. Vangchagya, E. Swatsitang, P. Thongbai, S. Pinitsoontorn, T. Yamwong, S. Maensiri, V. Amornkitbamrung, P. Chindaprasit, Very low loss tangent and high dielectric permittivity in Pure-CaCu<sub>3</sub>Ti<sub>4</sub>O<sub>12</sub> Ceramics prepared by a Modified Sol-Gel process. *J. Am. Ceram. Soc.* 95, 1497–1500 (2012)
12. P. Thongbai, T. Yamwong, S. Maensiri, V. Amornkitbamrung, P. Chindaprasit, Improved dielectric and nonlinear electrical properties of fine-grained CaCu<sub>3</sub>Ti<sub>4</sub>O<sub>12</sub> ceramics prepared glycine-nitrate process. *J. Am. Ceram. Soc.* 97, 1785–1790 (2014)
13. M.A. Dela Rubia, P. Leret, A. del Campo, R.E. Alonso, A.R. Lopez-Garcia, J.F. Fernandez, J. De Frutos, Dielectric behaviour of Hf-doped CaCu<sub>3</sub>Ti<sub>4</sub>O<sub>12</sub> ceramics obtained by conventional synthesis and reactive sintering. *J. Eur. Ceram. Soc.* 32, 1691–1699 (2012)
14. R. Schmidt, S. Pandey, P. Fiorenza, D.C. Sinclair, Non-stoichiometry in “CaCu<sub>3</sub>Ti<sub>4</sub>O<sub>12</sub>” (CCTO) ceramics. *RSC Adv.* 3, 14580–14589 (2013)
15. A. Nautiyal, C. Autret, C. Honstetter, S. De Almeida-Didry, M. El Amrani, S. Roger, B. Negulescu, A. Ruyter, Local analysis of the grain and grain boundary contributions to the bulk dielectric properties of Ca(Cu<sub>3–y</sub>Mg<sub>y</sub>)Ti<sub>4</sub>O<sub>12</sub> ceramics: importance of the potential barrier at the grain boundary. *J. Eur. Ceram. Soc.* 36, 1391–1398 (2016)
16. H. Yu, L.H. Liu, H. Hao, D. Luo, M. Cao, Dielectric properties of CaCu<sub>3</sub>Ti<sub>4</sub>O<sub>12</sub> ceramics modified by SrTiO<sub>3</sub>. *Mat. Lett.* 62, 1353–1355 (2008)
17. S. Rhouma, A. Megriche, M.E. Amrani, S. Said, S. Roger, C. Autret-Lambert, Effect of Sr/Mg co-doping on the structural, dielectric, and electrical properties of CaCu<sub>3</sub>Ti<sub>4</sub>O<sub>12</sub> ceramics. *J. Mater. Sci. Mater. Electron.* 33, 4535–4549 (2022)
18. Z. Peng, J. Li, P. Liang, Z. Yang, X. Chao, Improved dielectric properties and grain boundary response of SrTiO<sub>3</sub> doped Y<sub>2/3</sub>Cu<sub>3</sub>Ti<sub>4</sub>O<sub>12</sub> ceramics fabricated by Sol-gel process for high-energy-density storage applications. *J. Eur. Ceram. Soc.* 37, 4637–4644 (2017)

19. Z. Yang, L. Zhang, X. Chao, L. Xiong, J. Liu, High permittivity and low dielectric loss of the  $\text{Ca}_{1-x}\text{Sr}_x\text{Cu}_3\text{Ti}_4\text{O}_{12}$  ceramics. *J. Alloys Comp.* 509, 8716–8719 (2011)
20. R. Xue, D. Liu, Z. Chen, H. Dai, J. Chen, G. Zhao, Dielectric and Nonohmic Properties of  $\text{CaCu}_3\text{Ti}_4\text{O}_{12}/\text{SrTiO}_3$  Ceramics. *J. Electron. Mater.* 44, 1088–1094 (2015)
21. N. Kolev, R.P. Bontchev, A.J. Jacobson, V.N. Popov, V.G. Hadjiev, A.P. Litvinchuk, M.N. Iliev, Raman spectroscopy of  $\text{CaCu}_3\text{Ti}_4\text{O}_{12}$ . *Phys. Rev. B* 66, 132102 (2002)
22. A.F.L. Almeida, P.B.A. Fechine, M.P.F. Graca, M.A. Valente, A.S.B. Sombra, Structural and electrical study of  $\text{CaCu}_3\text{Ti}_4\text{O}_{12}$  (CCTO) obtained in a new ceramic procedure. *J. Mater. Sci. -Mater. Electron.* 20, 163–170 (2009)
23. J. Qu, F. Liu, X. Wei, C. Yuan, X. Liu, G. Chen, Q. Feng, X-ray diffraction, Dielectric, and Raman Spectroscopy Studies of  $\text{SrTiO}_3$ -Based microwave Ceramics. *J. Elect. Mater.* 45, 715–721 (2015)
24. S. Yoon, A.E. Maegli, L. Karvonen, S.K. Matam, A. Shk-abko, S. Riegg, T. Großmann, S.G. Ebbinghaus, S. Pokrant, A. Weidenkaff, Bandgap tuning in  $\text{SrTi}(\text{N},\text{o},\text{F})_3$  by anionic-lattice variation. *J. Solid State Chem.* 206, 226–232 (2013)
25. I. Norezan, A.K. Yahya, M.K. Talari, Effect of  $(\text{Ba}_{0.6}\text{Sr}_{0.4})\text{-TiO}_3$  (BST) doping on Dielectric Properties of  $\text{CaCu}_3\text{Ti}_4\text{O}_{12}$  (CCTO). *J. Mater. Sci. Technol.* 28, 1137–1144 (2012)
26. T.P. Gavrilovaa, J.A. Deevac, I.V. Yatsyk, A.R. Yagfarova, I.F. Gilmutdinov, N.M. Lyadov, F.O. Milovich, T.I. Chupakhinac, R.M. Eremina, Structural and magnetic properties of nanostructured composites  $(\text{SrFe}_{12}\text{O}_{19})_x(\text{CaCu}_3\text{Ti}_4\text{O}_{12})_{1-x}$ . *Phys. B: Condens Matter.* 536, 303–309 (2018)
27. R. Afindi Zaman, M. Johari Abu, M.F. Ab Rahman, W.F. F.W. ALL, J.J. Mohamed, M.F. Ain, Z.A. Ahmad, Dielectric Properties of  $\text{Al}_2\text{O}_3/\text{CaCu}_3\text{Ti}_4\text{O}_{12}$  Composite High frequency range. *Mater. Sci. Forum.* 288, 7–11 (2017)
28. S. DeAlmeida-Didry, C. Autret, A. Lucas, C. Honstetter, F. Pacreau, F. Gervais, Leading role of grain boundaries in colossal permittivity of doped and undoped CCTO. *J. Eur. Ceram. Soc.* 34, 3649–3654 (2014)
29. R. Mauczok, R. Wernicke, Ceramic boundary-layer capacitors. *Philips Tech. Rev.* 41, 338–346 (1983)
30. L. Marchin, S. Guillemet-Fritsch, B. Durand, A.A. Levchenko, A. Navrotsky, T. Lebey, Grain growth-controlled giant permittivity in soft chemistry  $\text{CaCu}_3\text{Ti}_4\text{O}_{12}$  ceramics. *J. Am. Ceram. Soc.* 91, 485–489 (2008)
31. W. Kobayashi, I. Terasaki,  $\text{CaCu}_3\text{Ti}_4\text{O}_{12}$  compos dielectrics: Ba/Pb-free dielectric ceram with high dielectric constants. *Appl. Phys. Lett.* 87, 032902 (2005)
32. H. Wu, Z. Zeng, S. Xing, M. Lan, W. Li, Q. Zhang, H. Ao, C. Zhou, R. Xu, R. Gao, X. Deng, Microstructure, Magnetodielectric, and Multiferroic Properties of  $x\text{Co}_{0.8}\text{Cu}_{0.2}\text{Fe}_2\text{O}_{4-y}$  ( $0.8\text{BaTiO}_3 - 0.2\text{BiAlO}_3$ ) Composite Ceramics. *Adv. Eng. Mater.* 23, 2100410 (2021)
33. H. X.Qin, C. Wu, H. Chen, W. Ao, R. Li, W. Gao, G. Cai, X. Chen, Z. Deng, X. Wang, C. Lei, Fu, Enhanced energy-storage performance of  $\text{Pb}_{0.925}\text{La}_{0.05}\text{Zr}_{0.95}\text{Ti}_{0.05}@x\text{wt}\%\text{SiO}_2$  composite ceramics. *J. Alloys Comp.* 890, 161869 (2022)
34. P. Thongbai, C. Masingboon, S. Maensiri, T. Yamwong, S. Wongsanmai, R. Yimmirun, Giant dielectric behavior of  $\text{CaCu}_3\text{Ti}_4\text{O}_{12}$  subjected to post-sintering annealing and uniaxial stress. *J. Phys. Condens. Matter.* 19, 236208 (2007)
35. P. Thongbai, J. Jumpatam, T. Yamwong, S. Maensiri, Effects of  $\text{Ta}^{5+}$  doping on microstructure evolution, dielectric properties and electrical response in  $\text{CaCu}_3\text{Ti}_4\text{O}_{12}$  ceramics. *J. Eur. Ceram. Soc.* 32, 2423 (2012)
36. P. Mao, J. Wang, L. He, L. Zhang, A. Annadi, F. Kang, Q. Sun, Z. Wang, H. Gong, Excellent capacitor – varistor properties in lead-free  $\text{CaCu}_3\text{Ti}_4\text{O}_{12}\text{-SrTiO}_3$  system with a Wrinkle structure via interface engineering. *ACS Appl. Mater. Interfaces* 43, 48781–48793 (2020)
37. J. Li, K.W.R. Jia, L. Hou, L. Gao, S. Li, Towards enhanced varistor property and lower dielectric loss of  $\text{CaCu}_3\text{Ti}_4\text{O}_{12}$  based ceramics. *Mater. Des.* 92, 92546–92551 (2016)
38. A. Nautiyal, C. Autret, C. Honstetter, S. Didry, M. El Amrani, S. Roger, Ruyter, dielectric properties of CCTO/MgTiO<sub>3</sub> composites: a new approach for capacitor application. *Int. J. Adv. Nanomater.* 1, 27–40 (2015)
39. R. Schmidt, D.C. Sinclair, K.N. Muller (eds.), *Capacitors: Theory of operation, behavior and safety regulations* (Nova Science Publishers Inc, New York, 2013)
40. J. Li, K. Wu, K. Jia, R. Hou, L. Gao, L. Li, Towards enhanced Varistor Property and Lower Dielectric loss of  $\text{CaCu}_3\text{Ti}_4\text{O}_{12}$  based Ceramics. *Mater. Des.* 92, 546–551 (2016)
41. S. Rhouma, S. Saïd, C. Autret, S. De Almeida-Didry, M. Amrani, Comparative studies of pure, Sr-doped, Ni-doped and co-doped  $\text{CaCu}_3\text{Ti}_4\text{O}_{12}$  ceramics: enhancement of dielectric properties. *J. Alloys Compd.* 717, 121–126 (2017)
42. J. Liu, C. Duan, W.N. Mei, R.W. Smith, J.R. Hardy, Dielectric properties and Maxwell-Wagner relaxation of compounds  $\text{ACu}_3\text{Ti}_4\text{O}_{12}$  ( $A = \text{Ca}, \text{Bi}_{2/3}, \text{Y}_{2/3}, \text{La}_{2/3}$ ). *J. Appl. Phys.* 98, 093703 (2005)
43. J.Y. Li, X.T. Zhao, S.T. Li, M.A. Alim, Intrinsic and extrinsic relaxation of ceramics: Effect of sintering. *J. Appl. Phys.* 108, 104104 (2010)
44. P. Thongbai, T. Yamwong, S. Maensiri, Non-ohmic and dielectric properties of  $\text{CaCu}_3\text{Ti}_4\text{O}_{12}\text{-MgO}$  nanocomposites. *Microelectron. Eng.* 108, 177–181 (2013)
45. S. De Almeida-Didry, M. Nomel, C. Autret, C. Honstetter, A. Lucas, F. Pacreau, F. Gervais, Control of grain boundary in alumina doped CCTO showing colossal permittivity by core-shell approach. *J. Eur. Ceram. Soc.* 38, 3182–3187 (2018)

46. S. Chung, I. Kim, S.L. Kang, Strong nonlinear current–voltage behaviour in perovskite-derivative calcium copper titanate. *Nat. Mater.* 3, 774–778 (2004)
47. T. Li, Z. Chen, Y. Su, L. Su, Effect of grain size and Cu-rich phase on the electric properties of  $\text{CaCu}_3\text{Ti}_4\text{O}_{12}$  ceramics. *J. Mater. Sci.* 44, 6149–6154 (2009)
48. L. Ramajo, R. Parra, J.A. Varela, M.M. Reboredo, M.A. Ramírez, M.S. Castro, Influence of vanadium on electrical and microstructural properties of  $\text{CaCu}_3\text{Ti}_4\text{O}_{12}/\text{CaTiO}_3$ . *J. Alloys Comp.* 497, 349–353 (2010)

**Publisher's Note** Springer Nature remains neutral with regard to jurisdictional claims in published maps and institutional affiliations.

Springer Nature or its licensor (e.g. a society or other partner) holds exclusive rights to this article under a publishing agreement with the author(s) or other rightsholder(s); author self-archiving of the accepted manuscript version of this article is solely governed by the terms of such publishing agreement and applicable law.